Volume 22
Number 7
18 February 2026
Pages 1475–1688

Soft Matter

rsc.li/soft-matter-journal

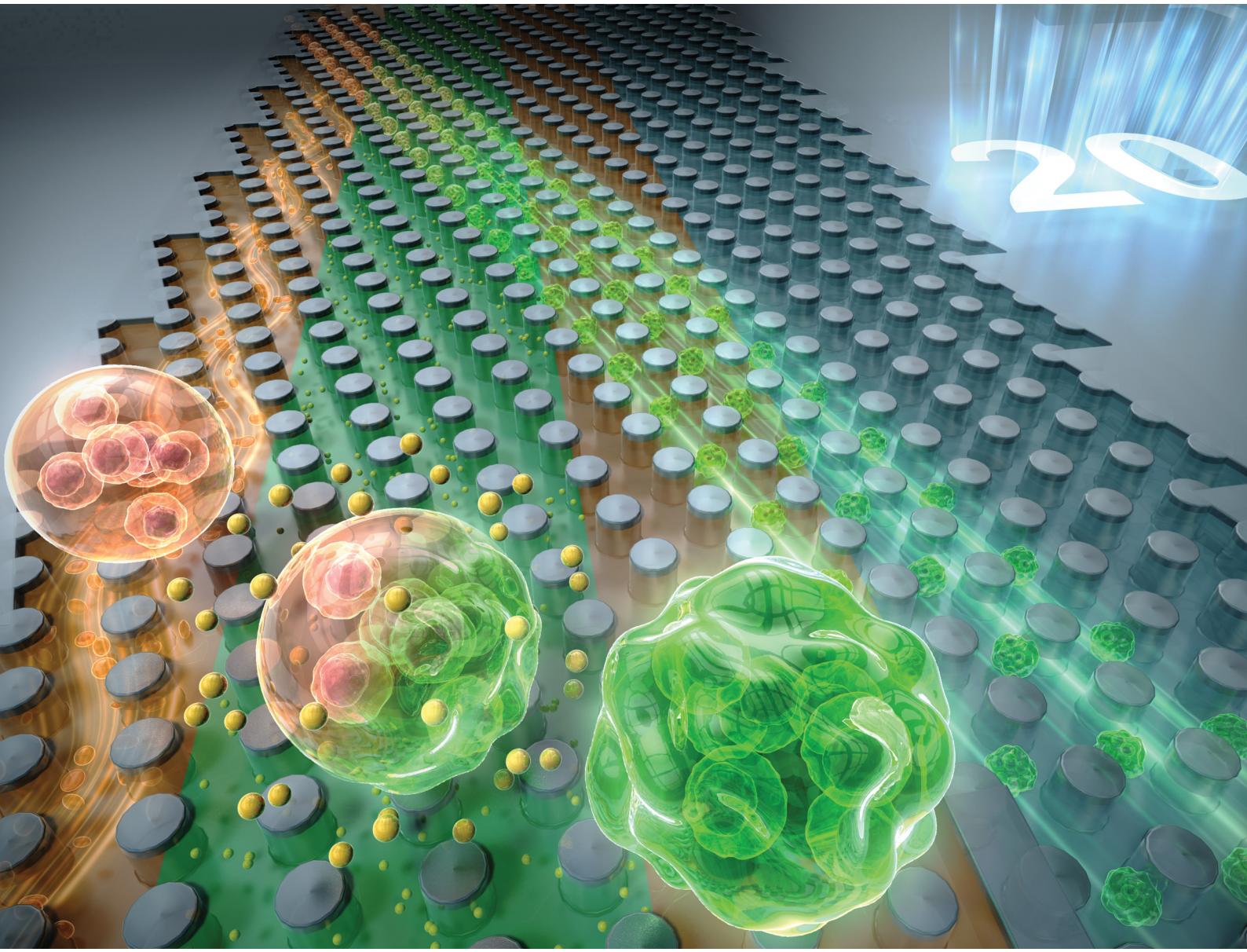

ISSN 1744-6848

ROYAL SOCIETY OF CHEMISTRY

PAPER
Takasi Nisisako *et al.*
Continuous production and extraction of monodisperse alginate microgels *via* deterministic lateral displacement

Soft Matter

PAPER

View Article Online
View Journal | View Issue

Cite this: *Soft Matter*, 2026, **22**, 1483

Continuous production and extraction of monodisperse alginate microgels *via* deterministic lateral displacement

Naotomo Tottori, †‡[a] Yeyi Tang, ‡[b] Yusuke Kanno [a] and Takasi Nisisako *[a]

Received 25th July 2025,
Accepted 29th November 2025

DOI: 10.1039/d5sm00757g

rsc.li/soft-matter-journal

Over the past two decades, microfluidic approaches have been extensively explored for the production of monodisperse alginate hydrogel microparticles, particularly for applications such as 3D *in vitro* cell culture in tissue engineering. However, conventional methods often suffer from satellite droplet contamination and inefficient oil-to-water phase transfer, limiting purity and scalability. Here, we present an integrated microfluidic platform for the continuous, on-chip production, gelation, extraction, and purification of monodisperse alginate hydrogel microparticles. The device combines a flow-focusing droplet generator with a deterministic lateral displacement (DLD) array, which guides alginate precursor droplets (mean diameter ~73 μm; CV ~2.7%) through a water-in-oil emulsion containing calcium ions to induce in-flow ionic crosslinking. The DLD array effectively separates gelled particles from satellite droplets (<37 μm) and transfers them across the oil–water interface into an aqueous stream, eliminating the need for off-chip centrifugation. We demonstrate the platform's applicability to cell encapsulation using MCF-7 cells, achieving a post-processing viability of ~80%. This work highlights the potential of integrating DLD-based trajectory control with in-flow chemical reactions to enable scalable, high-purity microparticle fabrication for biomedical applications.

Introduction

Alginate hydrogel microparticles have attracted considerable interest across a wide range of fields due to their excellent biocompatibility, mild gelation conditions, and ability to encapsulate diverse functional payloads. In pharmaceutical applications, they are used for controlled drug delivery, where alginate matrices enable sustained and localized release of therapeutic agents.[1,2] In biomedical research, they serve as 3D cell culture platforms for tissue engineering and high-throughput drug screening, offering immunoprotective yet permeable scaffolds for transplanted or cultured cells.[3,4] In the food and nutraceutical industries, these microparticles encapsulate probiotics, vitamins, and flavor compounds to enhance stability and enable targeted delivery.[5,6] They are also employed in environmental remediation and industrial biocatalysis as carriers for enzymes or microorganisms.[7,8] Across these applications, uniform particle size and morphology is essential, as it directly affects key performance metrics such as release kinetics, mass transfer, dosage accuracy, and mechanical integrity.

To address the demand for monodisperse particles, microfluidic technologies have been widely adopted over the past two decades for the production of alginate hydrogel microparticles.[9–11] In conventional approaches, alginate precursor droplets are typically generated *via* water-in-oil (W/O) emulsification using either shear-based (*e.g.*, T-junction or flow-focusing)[12–15] or interfacial-tension-driven (*e.g.*, microchannel emulsification[16–18]) systems. These droplets are then crosslinked with divalent cations—most commonly Ca^{2+}—to form hydrogels, either off-chip[14–17] or on-chip.[12,13,18] Gelation is achieved through either external[12,15,16,18] or internal[13,14,17] mechanisms. In external gelation, droplets are exposed to a surrounding solution containing Ca^{2+}, which diffuses inward to initiate crosslinking. Internal gelation, by contrast, involves co-encapsulation of calcium sources such as insoluble calcium carbonate ($CaCO_3$) nanoparticles[13,17] or water-soluble calcium-ethylenediaminetetraacetic acid (Ca-EDTA) complexes,[14] with gelation triggered by the diffusion of a slowly hydrolyzing acid (*e.g.*, acetic acid) from the continuous phase, leading to gradual *in situ* calcium release. While both approaches have been adapted to microfluidic formats, most systems still require downstream off-chip processes—such as oil-to-water phase transfer by centrifugation or removal of satellite particles by filtration—which increase workflow complexity, limit efficiency, and pose challenges for scalability.

[a] *Laboratory for Future Interdisciplinary Research of Science and Technology (FIRST), Institute of Integrated Research, Institute of Science Tokyo, R2-9, 4259 Nagatsuta-cho, Midori-ku, Yokohama 226-8501, Japan. E-mail: nisisako.t.aa@m.titech.ac.jp*

[b] *Department of Mechanical Engineering, School of Engineering, Institute of Science Tokyo, Tokyo 152-8550, Japan*

† Present address: Department of Mechanical Engineering, Faculty of Engineering, Kyushu University, Fukuoka, Japan.

‡ These authors contributed equally.

Several strategies have been explored for on-chip extraction of hydrogel microparticles from the oil phase into an aqueous phase,[19] each offering distinct advantages and limitations. Hydrodynamic filtration methods[20,21] employ mechanical filter gates or narrow side channels to facilitate phase transfer. While effective for alginate-based hydrogels, filtering structure in these systems need to be narrower than the particles for successful extraction, potentially causing increased clogging risk. Dielectrophoresis-based approaches exploit non-uniform electric fields to induce selective particle motion based on dielectric properties.[22] Although this technique enables high-resolution separation, its reliance on external energy sources adds complexity and limits scalability. Interfacial tension-driven methods leverage oil–water interface forces to transfer microgels into an aqueous phase.[23,24] However, these methods require selective surface patterning of the channel or strict control for a stable biphasic flow in the transfer section, making them difficult for scalable implementation.

Recently, deterministic lateral displacement (DLD) technology has emerged as a powerful method for passive, continuous, and size-based particle separation in microfluidic systems.[25] This technique employs a periodic array of micropillars to define a critical diameter, D_c, such that particles larger than D_c are laterally displaced along the array (bump mode), while smaller particles follow the streamline path (zigzag mode). Importantly, D_c is determined by the geometric parameters of the array and can be tuned to values significantly smaller than the inter-pillar gap, reducing the risk of clogging. Moreover, DLD separation is inherently independent of flow rates, making it robust and highly scalable. These advantages have led to its widespread use in separating both biological and synthetic particles. DLD platforms have also enabled precise particle trajectory control for applications such as the spatiotemporal chemical stimulation of cells migrating across laminar flow streams.[26] However, to date, DLD has not been applied to actively induce chemical reactions or facilitate phase transfer—such as on-chip ionic gelation and aqueous extraction of hydrogel microparticles—during particle transit.

In this study, we present a fully integrated microfluidic platform that enables continuous on-chip production, gelation, separation, and aqueous extraction of monodisperse alginate hydrogel microparticles (Fig. 1a). The system combines a flow-focusing microfluidic droplet generator (MFDG) with a downstream DLD array, which guides alginate precursor droplets through a calcium chloride emulsion stream for in-flow ionic crosslinking. The gelled particles are then separated from non-reactive satellite droplets and directed across the oil–water interface into a co-flowing aqueous stream. This integrated workflow eliminates the need for off-chip extraction steps such as centrifugation, offering a compact, scalable, and high-purity route for hydrogel microparticle fabrication. Furthermore, we demonstrate the platform's utility for biomedical applications by encapsulating MCF-7 cells and confirming high post-processing cell viability *via* live/dead fluorescence assays.

Experimental

Device design

We designed a microfluidic device that combines a flow-focusing MFDG with a DLD micropillar array for the continuous

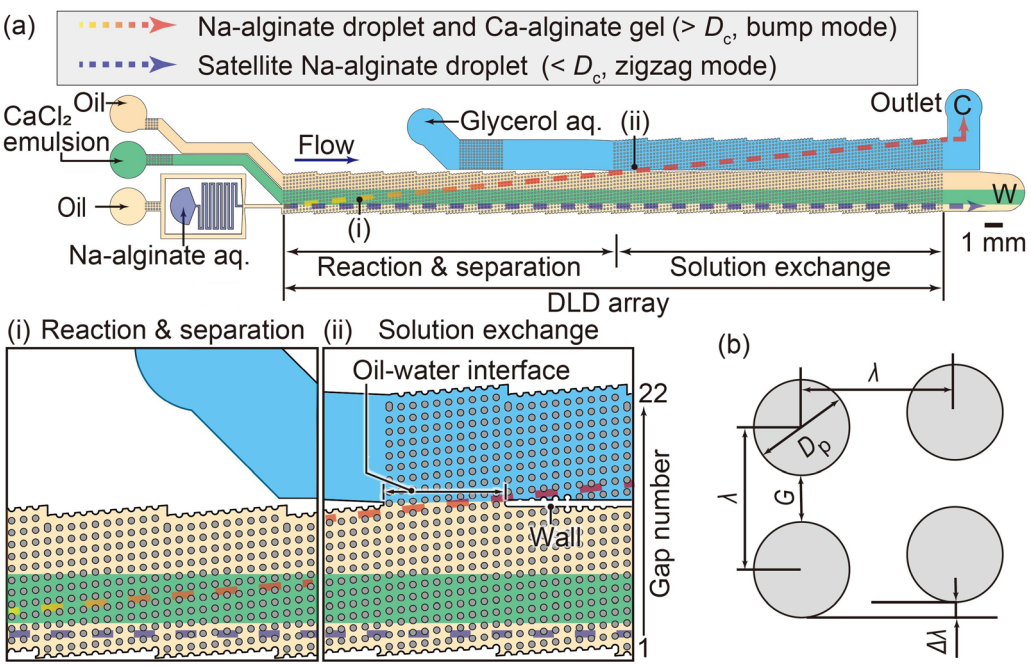

Fig. 1 Continuous production and aqueous extraction of monodisperse alginate hydrogel microparticles using a DLD micropillar array. (a) Schematic of the integrated microfluidic device. The inset highlights two functional regions: (i) ionic gelation of precursor droplets and removal of satellite droplets, and (ii) extraction of gelled microparticles from the oil phase into an aqueous phase. (b) Design parameters of the DLD array unit cell: pillar diameter (D_p) = 100 μm, array periodicity (λ) = 180 μm, displacement ratio ($\Delta\lambda/\lambda$) = 0.1, and gap width ($G = \lambda - D_p$) = 80 μm.

fabrication and purification of alginate hydrogel microparticles. The MFDG includes three inlet channels (each 100 μm wide) and a drain channel (200 μm wide). Downstream, the DLD array is composed of micropillars with a gap of G = 80 μm, pillar diameter D_p = 100 μm, and a row-to-row shift ratio of $\Delta\lambda/\lambda$ = 0.1 (Fig. 1b). Additional side channels are included for introducing gelation reagents and aqueous streams, enabling gelation and extraction within the same chip.

The DLD array consists of two functional regions: (i) a reaction and separation region, and (ii) a solution exchange region. In the first region, sodium alginate (Na-alginate) droplets encounter a side-flowing W/O emulsion containing calcium chloride ($CaCl_2$), initiating ionic crosslinking.[27] This zone consists of 10 sections, each comprising 10 columns and 12 rows. Droplets larger than D_c migrate laterally (bump mode) across the reactant stream, while smaller satellite droplets follow zigzag paths and are diverted away.[28,29]

In the subsequent solution exchange region, gelled microparticles are transferred from the oil phase into an aqueous phase. This region follows the same DLD principle but features an extended geometry—10 sections with 10 columns and 22 rows per section—to ensure thorough oil-to-water phase transfer. A physical barrier between sections 12 and 20 stabilizes the oil–water interface and reduces interfacial disturbance. The extended rows increase exposure time to the aqueous stream, enhancing washing and minimizing oil residue.

The D_c for size-based separation was estimated using the following empirical formula for binary separation:[25]

$$D_c = 1.4 \times G \times (\Delta\lambda/\lambda)^{0.48} \quad (1)$$

Substituting G = 80 μm and $\Delta\lambda/\lambda$ = 0.1 yields $D_c \sim 37$ μm, suitable for separating both precursor droplets and resulting gelled particles. Sidewall gaps were also optimized to minimize unwanted lateral drift during migration.[30]

Device fabrication

The microfluidic device was fabricated from polydimethylsiloxane (PDMS) using standard soft lithography (Fig. S1). For mold preparation, a negative photoresist (SU8-3050, Kayaku Advanced Materials, MA, USA) was spin-coated onto a silicon wafer at 1300 rpm to obtain a 100 μm-thick layer. The coated wafer was prebaked at 95 °C for 40 minutes to remove residual solvent and partially solidify the resist. Microchannel patterns were defined by UV exposure through a laser-printed polyethylene terephthalate (PET) photomask (thickness: 0.175 mm, resolution: 25 400 dpi; Unno Giken, Tokyo, Japan) using a mask aligner (MA-10, MIKASA, Tokyo, Japan). Post-exposure, the wafer was baked at 95 °C for 7 minutes to complete crosslinking, followed by development in SU-8 developer to reveal the relief patterns. To enhance mechanical durability, the mold was hard-baked at 150 °C for 7 minutes.

To facilitate PDMS demolding, the SU-8 mold was silanized in a sealed Petri dish with 0.5 mL of vaporized chlorotrimethylsilane (Tokyo Chemical Industry, Tokyo, Japan). PDMS prepolymer and curing agent (Toray, Tokyo, Japan) were mixed at a 10 : 1 (w/w) ratio, degassed, poured onto the mold, and cured at 80 °C for 1 hour. The cured PDMS layer was peeled off, and inlet/outlet holes (~1 mm diameter) were punched using a biopsy punch (Kai Industries, Gifu, Japan).

To construct a device with all internal surfaces composed of PDMS—unlike PDMS-glass bonded devices—a thin PDMS layer was spin-coated and cured on a glass slide (76 mm × 26 mm, thickness 0.9–1.2 mm), onto which the molded PDMS channel layer was bonded *via* oxygen plasma treatment (BP-1, Samco, Tokyo, Japan). This configuration ensured that the microchannel interior was entirely PDMS-lined, minimizing interfacial variability and undesired wall interactions.

Following assembly, the device was baked at 95 °C for 24 hours to promote hydrophobic recovery of PDMS surfaces. This step was critical for ensuring W/O droplet stability and minimizing particle/wall adhesion during droplet transport, without requiring surfactant additives or surface coatings.

To validate the applicability of the empirical formula for D_c (Eqn 1) under emulsion-rich conditions within our device, we conducted control tests comparing droplet migration behaviors in single-phase and multiphase flows (see the SI, Note S1 and Fig. S2 and S3).

Production of alginate microgels without cells

Unless otherwise noted, all chemicals were obtained from FUJIFILM Wako Pure Chemical Corporation (Osaka, Japan). To prepare the dispersed phase, Na-alginate (194-13321, Wako 1st Grade) was dissolved in ultrapure water (Direct-Q UV3, Merck, Hessen, Germany) to form a 3 wt% solution. This Na-alginate was selected for its specified viscosity (80–120 mPa s at 10 g L^{-1}, 20 °C); however, its molecular weight and mannuronic/guluronic acid (M/G) ratio were not provided by the manufacturer. The 3 wt% concentration was selected to ensure robust gelation upon contact with the calcium chloride emulsion and to maintain consistency with our previous microfluidic studies employing emulsion-based external gelation (EEG).[27,31] Corn oil was used as the continuous phase. The crosslinking reactant—a W/O emulsion containing $CaCl_2$—was prepared by dissolving 30 wt% $CaCl_2$ in ultrapure water and emulsifying it with corn oil containing 0.3 wt% surfactant (SY-Glyster CRS-75, Sakamoto Yakuhin Kogyo, Osaka, Japan) at an aqueous-to-oil volume ratio of 1 : 3. The emulsion was homogenized using a high-shear homogenizer (T10 basic ULTRA-TURRAX, IKA, Germany) to yield a stable W/O emulsion containing uniformly dispersed aqueous $CaCl_2$ droplets with an estimated average diameter of approximately 2 μm.[31] For the washing buffer solution, an 80 wt% glycerol solution in ultrapure water was prepared. The addition of glycerol increased the viscosity of the aqueous phase, helping to stabilize the oil–water interface during particle extraction and transfer within the device.

Production of cell-laden alginate microgels

MCF-7 cells (human breast adenocarcinoma cell line, RCB1904) were obtained from Riken BRC (Ibaraki, Japan) and cultured in Eagle's minimum essential medium (EMEM; Sigma-Aldrich, MO, USA) supplemented with 10% (v/v) fetal bovine serum

(FBS; MP Biomedicals, OH, USA), 1% (v/v) penicillin–streptomycin, 0.1 mM non-essential amino acids (NEAA), and 1 mM sodium pyruvate. Cells were maintained at 37 °C in a 5% CO_2 incubator (E-22, AS ONE, Osaka, Japan). Once cell cultures reached 80–90% confluence, they were harvested using 0.25% (w/v) trypsin–ethylenediaminetetraacetic acid (trypsin–EDTA) and resuspended for use in microparticle production.

To prepare the dispersed phase, 0.175 g of Na-alginate was dissolved in 4 mL of EMEM by stirring at 1400 rpm for 30 minutes at room temperature. Subsequently, 1 mL of the cell suspension was added to the alginate solution and stirred at 1400 rpm for an additional 30 seconds, resulting in a 3 wt% Na-alginate solution containing uniformly dispersed MCF-7 cells. The final cell concentration was approximately 4×10^6 cells mL^{-1}.

Corn oil was used as the continuous phase. The $CaCl_2$ emulsion was prepared by dissolving 30 wt% $CaCl_2$ in phosphate-buffered saline (PBS) and emulsifying it with corn oil containing 0.3 wt% surfactant (SY-Glyster CRS-75) at a 1 : 3 aqueous-to-oil volume ratio using a homogenizer. For the washing buffer, an 80 wt% glycerol solution in culture medium was prepared. After microfluidic production, the cell-laden alginate hydrogel microparticles were immediately collected into a Petri dish containing culture medium and transferred to a cell culture incubator for further processing or analysis.

Cell viability assay

To evaluate cell viability at various stages of the process—after standard 2D culture, after suspension in Na-alginate solution, and after microfluidic processing—dual fluorescent staining was performed using calcein-AM and propidium iodide (PI). Calcein-AM (C396, DOJINDO LABORATORIES, Kumamoto, Japan) stains viable cells green, while PI (C378, DOJINDO LABORATORIES) stains dead cells red.

Prior to the DLD experiment, MCF-7 cells were assessed for viability after standard 2D culture and after dilution into a 3 wt% Na-alginate solution prepared in cell culture medium. For each condition, 10 μL each of calcein-AM and PI solutions were added to 1 mL of the cell suspension and incubated at 37 °C under 5% CO_2 for 30 minutes. The stained samples were imaged using an inverted microscope (IX71; Evident, Tokyo, Japan) equipped with fluorescent filter sets (U-MWBS3 for calcein-AM and U-MWIG2 for PI; Evident) and a color camera (SC2003; SWIFTCAM, Hong Kong, China). Overlay images of the fluorescence channels were generated using ImageJ software (NIH, NY, USA).

To assess the impact of microfluidic processing, 1 mL of the collected hydrogel microparticle suspension was stained immediately after collection using the same staining protocol, and imaged with the same microscopy setup.

For long-term culture experiments, the remaining cell-laden alginate hydrogel microparticles were transferred into a standard culture dish and incubated at 37 °C in a humidified 5% CO_2 atomosphere. The culture medium was replaced every two days by aspirating the supernatant and gently adding fresh medium. At specified time points (days 1, 3, 5, 7, and 9), 1 mL of the microparticle suspension was retrieved after gentle agitation of the dish to evenly distribute the beads. The samples were stained with 10 μL each of calcein-AM and PI, incubated for 30 minutes under standard conditions, and then imaged using the same microscope and camera system. Fluorescent overlays were prepared using ImageJ.

Peripheral equipment and procedure

Gastight glass syringes (1000 Series; Hamilton Company, Reno, NV, USA) were pre-filled with the required liquids and connected to the PDMS microfluidic device *via* polyethylene tubing (outer diameter, 1 mm; inner diameter, 0.5 mm). Fluids were precisely infused into the device using syringe pumps (KDS200 and Legato 180, KD Scientific, MA, USA) to maintain a stable and controlled flow rate. Droplet formation at the MFDG and subsequent trajectories within the DLD array were observed and recorded using an inverted optical microscope (IX73, Evident) equipped with a high-speed video camera (Fastcam Mini AX50, Photron, Tokyo, Japan). Video frames were analyzed using ImageJ to assess droplet sizes and light-intensity distribution within the microchannel. The dimensions of the collected alginate hydrogel particles, including diameter and roundness, were evaluated by manually tracing their boundaries. Solution viscosities at 25 °C (Table S1) were measured using a vibratory viscometer (Viscomate VM-10A-L; Sekonic, Tokyo, Japan), and interfacial tensions at the oil–water interface (Table S2) were measured using a pendant-drop method with a contact angle meter with a pendant-drop method (B100; Asumi Giken, Tokyo, Japan).

Results and discussion

Production of alginate microgels without cells

The formation of Na-alginate droplets within the MFDG was initially investigated. As shown in Fig. 2a, droplet generation occurred in the dripping regime at a single MFDG, with flow rates set to 4.0 mL h^{-1} for the continuous phase (Q_c) and 0.005 mL h^{-1} for the dispersed phase (Q_d). Under these conditions, droplet pinch-off occurred at a rate of approximately 8 droplets per second, corresponding to a production rate of $\sim 2.9 \times 10^4$ droplets per hour. Following the detachment of each main droplet, a series of smaller satellite droplets formed from a thinning fluid filament *via* Plateau-Rayleigh instability (Fig. 2a, inset). To suppress the formation of such satellite droplets, droplet generation was maintained in the dripping regime, which avoids the extended fluid threads characteristic of the jetting regime that typically promote satellite droplet formation.

Fig. 2b shows the size distributions of both main and satellite droplets. The main droplets exhibited a mean diameter of 73 ± 2 μm with a coefficient of variation (CV) of 2.7%, indicating excellent monodispersity. In contrast, the satellite droplets displayed a broader size distribution and were classified into distinct size groups. The largest satellite droplets (primary satellites) had an average diameter of 25 ± 3 μm. Given these results, the DLD array's D_c of approximately 37 μm was expected to be well-suited for separating main droplets from satellite droplets within the device.

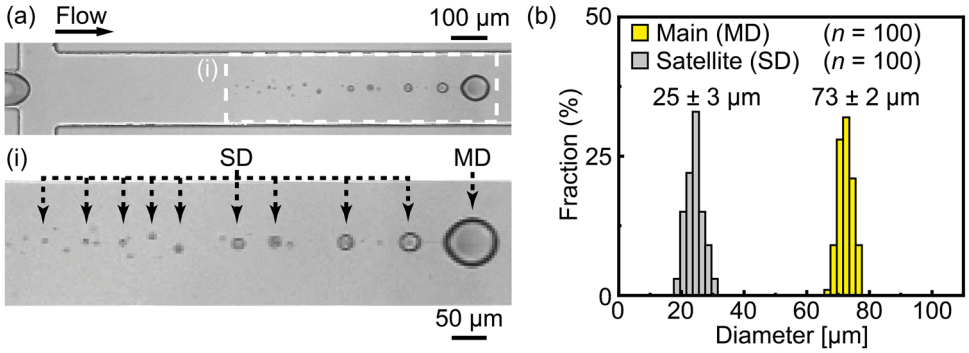

Fig. 2 Generation of main and satellite sodium alginate droplets in the flow-focusing droplet generator. (a) High-speed photomicrograph (13600 fps) showing the formation of a main droplet followed by satellite droplets. Flow rates: continuous phase (Q_c) = 4.0 mL h^{-1}; dispersed phase (Q_d) = 0.005 mL h^{-1}, respectively. Under these conditions, the main droplets formed at a rate of approximately 8 droplets per second. (b) Size distributions of the main and primary satellite droplets.

Following droplet formation, the droplets entered the DLD array near the right sidewall (gap number: 3) while remaining within the primary fluid stream. The flow rates of the reactant phase ($CaCl_2$ emulsion), oil phase, and washing aqueous buffer solution were set to 4.0 mL h^{-1}, 3.5 mL h^{-1}, and 15.0 mL h^{-1}, respectively. Upon entering the DLD array, the Na-alginate main droplets (mean diameter ~73 μm), which were larger than D_c of approximately 37 μm (see SI Note S1), migrated in bump mode, gradually shifting laterally along the designed pillar arrangement (Fig. 3a and Video S1). During this migration, the main droplets traversed the $CaCl_2$ emulsion stream for approximately 0.6 s, facilitating hydrogel formation *via* external

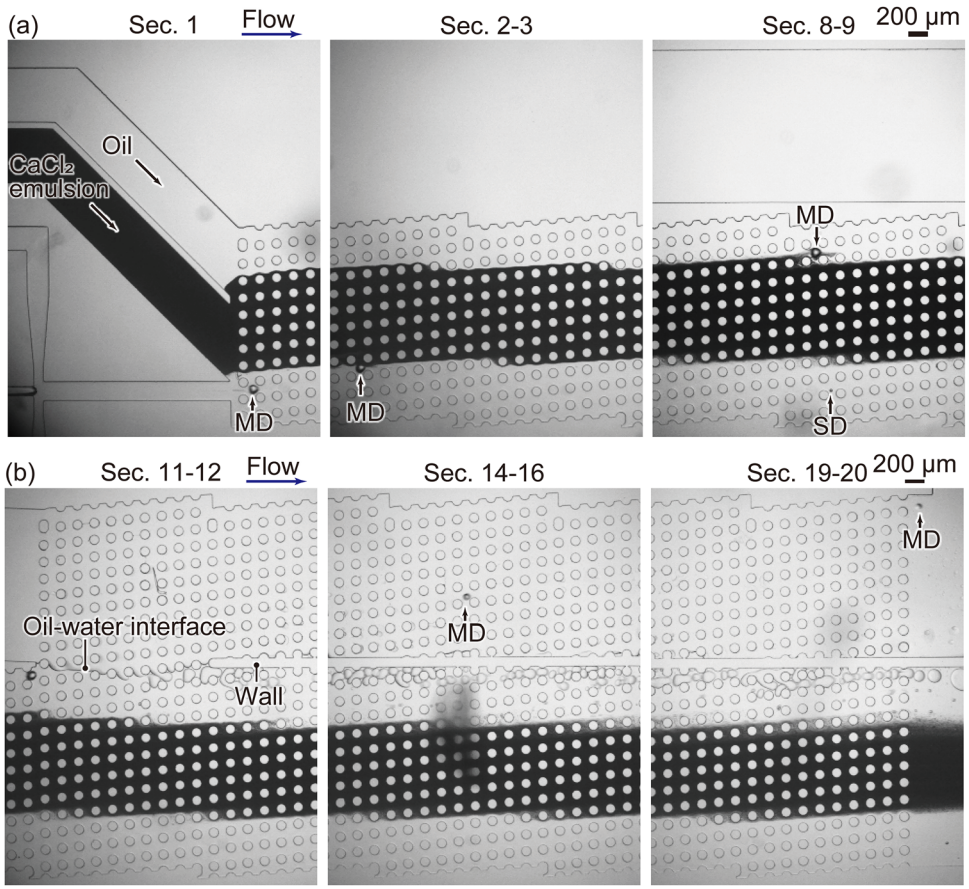

Fig. 3 On-chip production and extraction of alginate hydrogel microparticles. (a) Gelation of sodium alginate droplets as they traverse a $CaCl_2$-containing emulsion stream in the DLD array. Images show droplet progression at selected array sections: section 1, sections 2–3, and sections 8–9. (b) Aqueous extraction of gelled microparticles through the oil–water interface within the DLD array. Representative images show microparticle transition at sections 11–12, 14–16, and 19–20.

gelation. Calcium ions from the $CaCl_2$ emulsion diffused into the Na-alginate droplets through coalescence, initiating crosslinking. In contrast, the satellite droplets, which were smaller than D_c, followed the zigzag mode, remaining within the primary fluid stream without significant lateral displacement and were ultimately collected at the waste outlet (outlet W).

After passing through the separation and reaction region, the crosslinked alginate hydrogel particles crossed the oil–water interface, leading to their extraction into the aqueous phase. Following extraction, the alginate hydrogel particles continued migrating in bump mode, underwent washing, and were finally collected at the designated product outlet (outlet C) (Fig. 3b and Video S1). When the crosslinked microgels crossed the oil–water interface, they initially contacted the interface and were transferred into the aqueous phase within ~4 ms. The extraction efficiency of hydrogel particles was measured at 98%, confirming the effectiveness of the separation process. Although minor flow disturbances and secondary droplet formation were observed in the aqueous phase near the oil–water interface (section 11), the extracted hydrogel particles resumed lateral migration in bump mode (Fig. 4a). As the particles moved downstream, the peaks of their light-intensity profile across the cross-section gradually decreased, suggesting effective washing and equilibration with the surrounding aqueous solution (Fig. 4b). Overall, the system achieved a particle throughput of approximately 2.8×10^4 microgels per hour, demonstrating the platform's potential for scalable production.

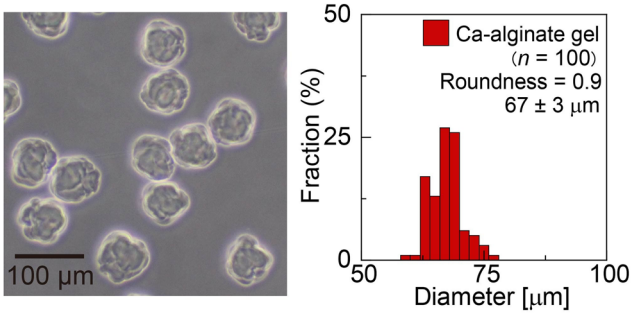

Fig. 5 Photomicrograph of alginate hydrogel microparticles collected at outlet C and their size distribution.

Post-extraction analysis of the hydrogel particles confirmed successful recovery into the aqueous phase (Fig. 5). The particles exhibited a mean diameter of 67 ± 3 μm and a roundness value of 0.9, indicating high monodispersity and sphericity. Compared to the precursor droplets, the microgels showed slight shrinkage and "raisin-like" surface texture. Additional control experiments (Fig. S4) showed that microgels collected directly in corn oil—without passing through the extraction phase—retained a smoother surface, suggesting that the roughness observed here originated from osmotic imbalance and interfacial stresses during transfer across the glycerol-rich aqueous extraction phase. While inhomogeneous gelation inherent to external gelation[4]

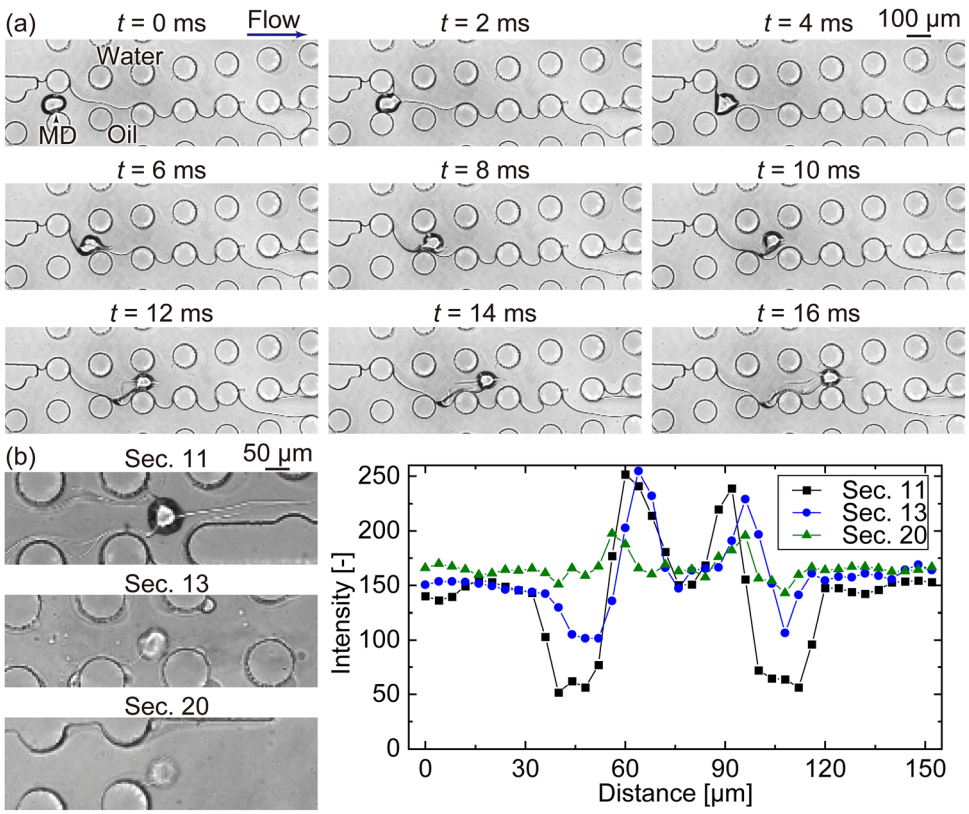

Fig. 4 Dynamics of microgel extraction through the oil–water interface. (a) Time-lapse images showing an alginate microgel crossing the oil–water interface. (b) Light-intensity profiles of a microgel recorded at different DLD sections (section 11, section 13, section 20), illustrating changes during extraction.

likely contributes, these results indicate that further optimization of the extraction medium, particularly its osmolarity, may help improve surface morphology in future implementations.

Furthermore, we systematically varied Q_c and Q_d to identify the operational conditions for successful microgel synthesis and collection, as well as to assess the achievable size range of the resulting microgels. The outcomes are summarized in a Q_c–Q_d phase diagram (Fig. S5). The region of successful microgel synthesis (Region A) was observed for Q_c ranging from 2.0 to 5.0 mL h^{-1} and Q_d from 0.005 to 0.010 mL h^{-1}. At excessively high Q_c values, the resulting precursor droplets were smaller than D_c, leading to zigzag-mode migration and unsuccessful gelation (region C). Conversely, when Q_c was too low or Q_d was too high, the increased number or size of droplets resulted in frequent clogging within the DLD array (region B). Within the successful region, the largest microgels (91 ± 4 μm) were obtained at Q_c = 2.0 mL h^{-1} and Q_d = 0.010 mL h^{-1} (Fig. S6), while the smallest microgels (56 ± 2 μm) were obtained at Q_c = 5.0 mL h^{-1} and Q_d = 0.005 mL h^{-1} (Fig. S7).

Production of cell-laden alginate microgels

Prior to conducting the DLD experiment for the production of cell-laden alginate hydrogel microparticles, we evaluated the viability of MCF-7 cells before and after dilution in a 3 wt% Na-alginate solution prepared in cell culture medium. Fig. S8a shows representative bright-field and fluorescence microscopy images of the cells (average diameter: 17 ± 3 μm) following standard 2D culture. A high proportion of viable cells (green) was observed, with only a small fraction of dead cells (red), yielding a viability of 97.5% (Fig. S8b). In contrast, upon suspension in the 3 wt% alginate solution, a slight increase in dead cells was observed (Fig. S8c), with the quantified viability decreasing modestly to 91.5% (Fig. S8d). This minor reduction is likely due to mechanical stress induced by the increased viscosity of the alginate solution during the mixing process.

Cell-laden alginate hydrogel particles were produced following the same protocol as for the particles without cells. Na-alginate precursor droplets containing MCF-7 cells were reliably generated in the flow-focusing MFDG under identical flow conditions (Q_c = 4.0 mL h^{-1}, Q_d = 0.005 mL h^{-1}). Under these conditions, the main precursor droplets exhibited an average diameter of 98 ± 1 μm, while the largest satellite droplets measured 28 ± 3 μm on average (Fig. S9), enabling effective size-based separation by the DLD array designed with D_c = 37 μm. The generation rate of main droplets was approximately

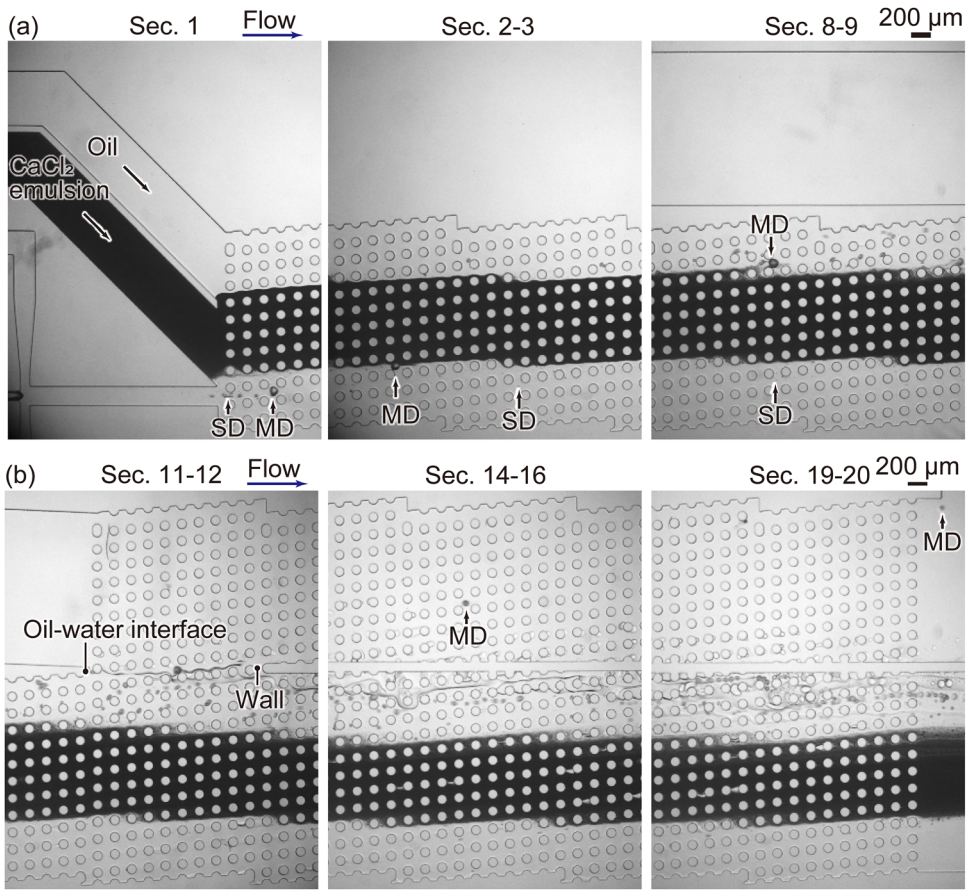

Fig. 6 On-chip production and extraction of cell-laden alginate hydrogel microparticles. (a) Gelation of MCF-7 cell-laden droplets within the $CaCl_2$ emulsion stream inside the DLD array. Images captured at sections, 1, 2–3, and 8–9. (b) Aqueous extraction of the gelled, cell-laden microparticles *via* the oil–water interface. Images correspond to sections 11–12, 14–16, and 19–20.

3 droplets per second, corresponding to a production rate of $\sim 1.1 \times 10^4$ droplets per hour. Both main and satellite droplets entered the DLD array near the right sidewall (gap number: 3), and the flow rates of the reactant phase, oil phase, and aqueous washing buffer were maintained at 4.0 mL h^{-1}, 3.5 mL h^{-1}, and 15.0 mL h^{-1}, respectively.

The cell-laden Na-alginate main droplets (mean diameter $\sim$100 μm) migrated in bump mode, shifting laterally and crossing the $CaCl_2$ emulsion stream within $\sim$0.6 s, leading to hydrogel formation (Fig. 6a and Video S2). Similar to the previous experiment, Ca^{2+} ions diffused into the droplets, triggering external gelation. Satellite droplets, being smaller than D_c, followed the zigzag mode and collected at outlet W.

After passing through the separation and reaction region, the crosslinked cell-laden alginate particles crossed the oil–water interface (Fig. 6b and Video S2), leading to their extraction into the aqueous phase within $\sim$4 ms. The extraction efficiency in this case was measured at 73%, which was lower than that of the hydrogel particles without cells. This reduction in extraction efficiency may have resulted from differences in solution composition, as cell culture medium was used to dissolve Na-alginate and glycerol, while PBS served as the solvent for $CaCl_2$. Such variations in medium composition could have influenced the interfacial tension at the oil–water boundary, thereby reducing extraction efficiency.

To investigate the reduced extraction efficiency observed for cell-laden microgels compared to cell-free ones, we examined the interfacial tension between the oil phase (corn oil) and various aqueous phases. As summarized in Table S2, the interfacial tension between corn oil and 3 wt% Na-alginate in pure water was 6.8 ± 0.2 mN m^{-1}, whereas it decreased to 3.7 ± 0.1 mN m^{-1} when the alginate solution was prepared with EMEM. Similarly, the interfacial tension between corn oil and the extraction phase decreased from 17.5 ± 0.2 mN m^{-1} for 80 wt% glycerol in pure water to 13.2 ± 0.5 mN m^{-1} when EMEM was included. These results indicate that EMEM-based aqueous solutions lower the interfacial tension at the oil–water interface, which likely contributes to more stable interfaces and reduced transfer and extraction efficiency for cell-laden microgels.

As observed previously, flow disturbances and secondary droplet formation near the oil–water interface (section 11) were present. However, once extracted, the hydrogel particles resumed bump mode migration within the aqueous phase (Fig. S10a). As the particles moved downstream, the peaks of their light-intensity distribution gradually decreased, indicating efficient washing and equilibration with the buffer solution (Fig. S10b). Under these conditions, the system achieved a throughput of approximately 7.9×10^3 microgels per hour.

Fig. 7a shows a bright-field microscopy image of the cell-laden alginate hydrogel microparticles immediately after off-chip collection. The particles exhibited a mean diameter of 101 ± 2 μm and a roundness value of 0.95 (Fig. 7b), indicating that they were highly monodisperse and spherical, reflecting the uniformity of the precursor Na-alginate droplets. Unlike the particles without cells shown earlier (Fig. 5a), the cell-laden particles had larger diameters, closely matching those of the precursor droplets, and displayed smooth surface morphology. This difference is likely due to the osmotic buffering capacity of

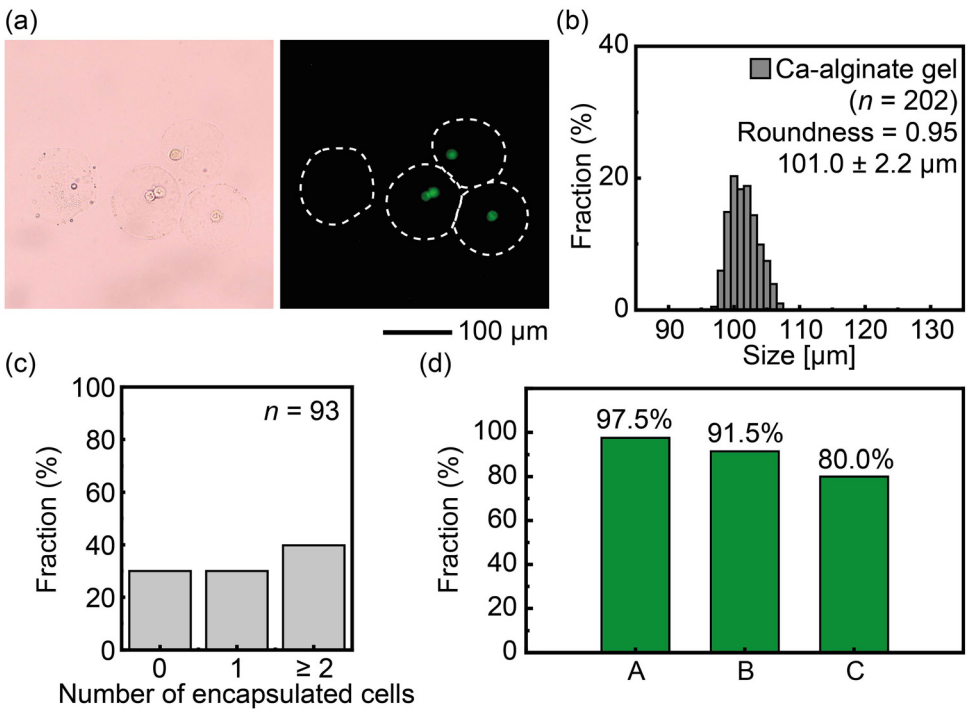

Fig. 7 Characterization of cell-laden alginate hydrogel microparticles after off-chip collection. (a) Bright-field and fluorescence microscopy images showing encapsulated cells. (b) Distribution of microparticles by the number of encapsulated cells. (c) Size distribution of the cell-laden microparticles. (d) Cell viability data after (A) 2D culture, (B) dilution in alginate solution, and (C) encapsulation.

the culture medium (EMEM), which was used in both the dispersed phase and extraction phase. The presence of solutes in EMEM likely mitigates osmotic pressure gradients during gelation, thereby reducing dehydration or shrinkage and helping preserve particle morphology.

Cell loading statistics revealed that approximately 30% of the particles were empty, 30% contained a single cell, and 40% encapsulated multiple cells (Fig. 7c). The viability of the encapsulated cells was measured at 80.0%, representing a moderate decrease compared to the viability observed before microfluidic processing (91.5%) (Fig. 7d). This reduction is likely attributable to the encapsulation process itself. While alginate hydrogels are generally considered biocompatible and protective, they may impose limitations on nutrient diffusion or create localized variations in pH and oxygen levels. Additionally, since the DLD experiment was conducted at room temperature, temperature fluctuations relative to physiological conditions may have contributed to cell stress and the loss of viability in more sensitive cells.

To evaluate the long-term viability and proliferation potential of encapsulated cells, cell-laden alginate hydrogel microparticles were recultured under standard conditions, and their viability was assessed on days 1, 3, 5, 7, and 9 using calcein-AM and PI staining (Fig. 8 and Fig. S11). On day 1, most encapsulated cells exhibited strong green fluorescence, indicating high viability. This trend continued through day 3, with a majority of cells remaining viable. However, by day 5, the number of red fluorescent (dead) cells had markedly increased. Viability continued to decline over time, and by day 9, all observed cells were non-viable (Fig. 9). Throughout the culture period, no significant proliferation of individually encapsulated cells was detected. Nevertheless, small spheroidal structures were occasionally observed within microparticles that initially encapsulated multiple cells. These findings suggest that while the hydrogel environment preserves short-term viability, it is insufficient to support sustained proliferation. This limitation is likely due to the use of unmodified alginate, which lacks cell-adhesive moieties necessary for attachment, spreading, and growth. Incorporation of bioactive components, such as collagen, gelatin, and chitosan,[4] or the use of a chemically modified alginate[14] may be necessary to promote long-term viability and proliferation within the matrix.

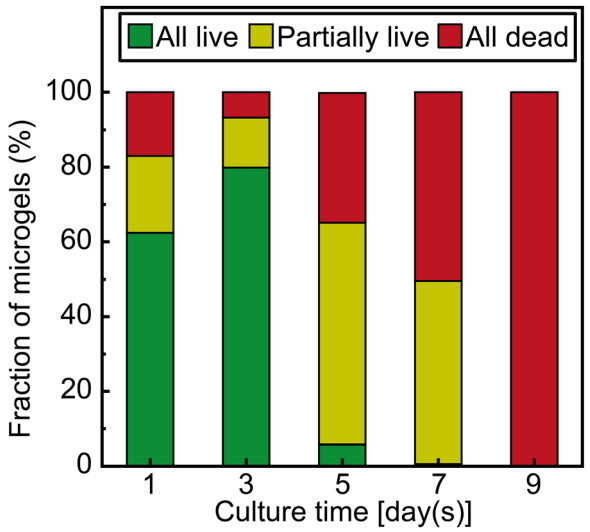

Fig. 9 Temporal change in cell viability states within alginate hydrogel microparticles during reculture, shown as fractional composition. "All live" indicates that all encapsulated cells within a given microparticle were viable; "Partially live" denotes microparticles containing a mix of live and dead cells; "All dead" refers to microparticles in which all encapsulated cells were non-viable.

Technical considerations and future directions

A key feature of the integrated system developed in this study is the use of the EEG method,[27,31] in which an oil-dispersed calcium chloride emulsion serves as the crosslinking reactant. While alternative strategies—such as external gelation using calcified oil[32] or internal gelation *via* pH-triggered calcium release[13,14,17]—are also viable, EEG was selected here for its ability to clearly visualize and control the spatial interaction between precursor droplets and the reactant stream. However, EEG requires physical contact and coalescence between the precursor droplet and calcium-containing microemulsion, which limits the use of surfactants prior to gelation. In densely packed systems, this can lead to

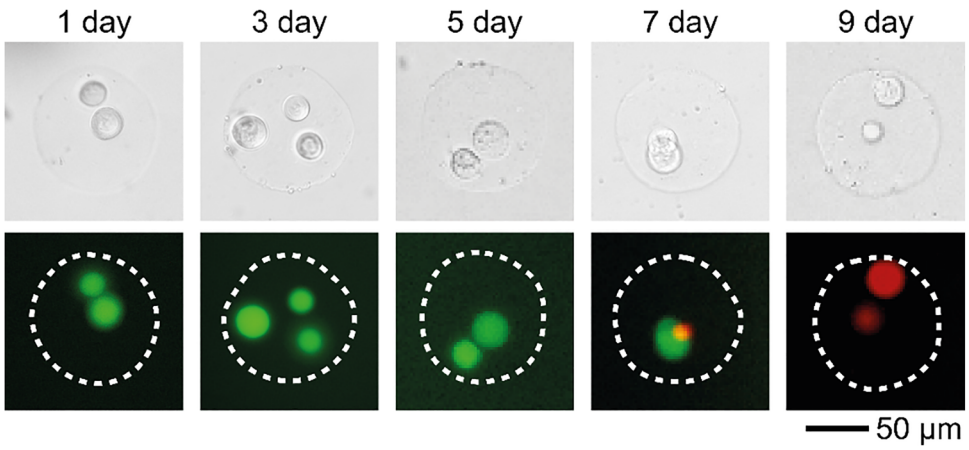

Fig. 8 Magnified bright-field and fluorescence microscopy images of encapsulated MCF-7 cells on days 1, 3, 5, 7, and 9 of reculture.

droplet coalescence and reduced monodispersity, ultimately constraining throughput. Additionally, gradual coalescence within the calcium emulsion over time destabilized the reactant phase, restricting continuous operation to a few hours. These limitations highlight the need for further optimization of emulsion stability to enable longer-term, higher-throughput applications.

Alternative gelation strategies may help address these challenges. Surfactant-compatible external gelation or internal gelation using chelated calcium sources offer promising routes to suppress coalescence. While earlier internal gelation methods often required acidic conditions to trigger calcium release—raising concerns about local cytotoxicity—recent advancements now enable internal gelation under pH-controlled, more physiologically relevant conditions.[33] Such developments may offer viable alternatives for biocompatible, continuous microgel production without the stability issues associated with EEG.

Another practical limitation identified in this study relates to precursor droplet generation. Due to the high viscosity of the 3 wt% Na-alginate solution, droplet production using a single MFDG was limited to several droplets per second. While employing lower-viscosity alginate solutions (*e.g.*, 1–2 wt%) could enhance droplet generation rates and reduce satellite droplet formation, such adjustments would require careful re-optimization of the device geometry–particularly the DLD array–to handle increased droplet volume fractions without inducing coalescence. In particular, fine-tuning the interpillar gap G and array gradient $\Delta\lambda/\lambda$ would be essential to ensure an appropriate D_c for effective satellite droplet removal.[28] Furthermore, the reduced extraction efficiency observed for cell-laden microgels compared to cell-free ones imposes an additional constraint on the overall throughput of the system.

To overcome these limitations, future work could explore the integration of parallelized droplet generators, such as shear-based MFDGs arranged in multi-nozzle arrays[34] or scalable step-emulsification modules.[35] These upstream components could be modularly connected to the current reaction–separation–extraction system, enabling higher-throughput microgel synthesis while maintaining monodispersity under controlled droplet/particle volume fractions. Additionally, co-flow stabilization strategies, surfactant compatibility, and emulsion phase optimization would further contribute to the robustness and scalability of the platform.

In addition to alginate, the platform may be extended to other hydrogel-forming materials that undergo ionic crosslinking, such as gellan gum, carrageenan, pectin, and chitosan-based hydrogels.[11] To explore this possibility, we conducted preliminary experiments using pectin as a model material. While we successfully observed pectin droplet generation, satellite droplet removal, and traversal through the calcium-containing emulsion stream (Fig. S12), stable off-chip recovery of the resulting microgels was not achieved—likely due to insufficient gelation under the tested conditions. These findings suggest that, although the platform conceptually supports diverse gel systems, successful application to non-alginate materials will require careful optimization of device geometry, flow conditions, and material formulations. Therefore, the platform's broader compatibility remains a promising but exploratory direction, with further development necessary to tailor the system for each specific hydrogel chemistry.

In addition to the droplet/particle sizes, their mechanical properties—particularly stiffness and deformability—can also modulate separability in DLD principle.[25] Soft or partially crosslinked beads may deform under shear stress during migration, reducing their apparent hydrodynamic size and potentially enabling them to pass through the array in zigzag mode, even if their undeformed size exceeds D_c. To minimize such deformation effects and maintain separation based strictly on geometric criteria, we conducted the experiments under relatively low shear conditions. From an alternative perspective, exploiting deformability-based separation could enable selective fractionation of microgels by their crosslinking degree or mechanical stiffness, which may be valuable in certain biomedical or materials science applications. These considerations suggest that both size and mechanical properties must be jointly optimized for high-fidelity separation in future implementations of our platform.

Finally, although this study primarily focused on functional validation, the system also offers a promising framework for precise tuning of gelation dynamics. By adjusting factors such as the DLD array angle, reactant stream width, and flow rate of the continuous phase, the duration of droplet exposure to the crosslinker (*i.e.*, the reaction time) can be modulated. Such control may allow fine control over internal microparticle morphology. For instance, it could enable the formation of core–shell structures with a liquified core and tunable shell thickness,[36] or facilitate the adjustment of mechanical properties of application-specific requirements. One future objective is to assess the range of mechanical stiffness that can be achieved using this platform, particularly in the context of encapsulating cell types sensitive to mechanical stress. Furthermore, multistream laminar co-flow designs may allow the fabrication of hybrid or composite microgels (*e.g.*, core–shell particles composed of alginate and other biopolymers).[37] Overall, this work establishes a robust platform for integrating multiple microfluidic operations and highlights its potential for expanded use in engineered hydrogel systems and biomedical manufacturing.

Conclusions

In this study, we developed a fully integrated microfluidic platform for the continuous production, gelation, separation, and extraction of monodisperse alginate hydrogel microparticles. The device combines a flow-focusing MFDG with a DLD micropillar array, enabling precise trajectory control of alginate precursor droplets. This design allows in-flow ionic crosslinking and effective separation from satellite droplets, followed by direct on-chip extraction of gelled particles into an aqueous phase. The resulting hydrogel microparticles exhibited a narrow size distribution (mean diameter $\sim$67 μm; CV $\sim$4.5%) and minimal contamination, eliminating the need for off-chip purification. We further demonstrated the applicability of the platform for cell encapsulation using MCF-7 cells. High post-processing viability confirmed the biocompatibility of the

method and its suitability for biomedical applications. Overall, this work demonstrates the utility of integrating DLD-based separation with in-flow chemical reactions for compact, scalable, and high-purity microparticle fabrication. The approach holds promise for broad applications in materials science, biomedicine, and drug delivery, and is readily adaptable to other hydrogel systems and encapsulation strategies.

Conflicts of interest

The authors declare no competing interests.

Data availability

The datasets generated during and/or analyzed during the current study are available from the corresponding author upon reasonable request.

The data supporting this article have been included as part of the supplementary information (SI). Supplementary information is available. See DOI: https://doi.org/10.1039/d5sm00757g.

Acknowledgements

This work was partially supported by JSPS KAKENHI Grant Numbers 19K23585, 20K21104.

References

1 A. Sosnik, *ISRN Pharmaceutics*, 2014, 926157.
2 D. M. Hariyade and N. Islam, *Adv. Phamacol. Pharmaceutical Sci.*, 2020, 8886095.
3 B. Namgung, K. Ravi, P. P. Vikraman, S. Sengupta and H. L. Jang, *Biochem. Soc. Trans.*, 2021, **49**, 761–773.
4 S.-M. Kang, J.-H. Lee, Y. S. Huh and S. Takayama, *ACS Biomater. Sci. Eng.*, 2021, **7**, 2864–2879.
5 A. Łętocha, M. Miastkowska and E. Sikora, *Polymers*, 2022, **14**, 3834.
6 X. Wang, S. Gao, S. Yun, M. Zhang, L. Peng, Y. Li and Y. Zhou, *Pharmaceuticals*, 2022, **15**, 644.
7 Y. Weng, G. Yang, Y. Li, L. Xu, X. Chen, H. Song and C.-X. Zhao, *Adv. Colloid Interface Sci.*, 2023, **318**, 102957.
8 H. Yamaguchi and M. Miyazaki, *Molecules*, 2024, **29**, 2021.
9 M. Yamada and M. Seki, *J. Chem. Eng. Jpn.*, 2018, **51**, 318–330.
10 C. Zhang, R. Grossier, N. Candoni and S. Veesler, *Biomater. Res.*, 2021, **25**, 41.
11 A. Moreira, J. Carneiro, J. B. L. M. Campos and J. M. Miranda, *Microfluid. Nanofluid.*, 2021, **25**, 10.
12 H. Shintaku, T. Kuwabara, S. Kawano, T. Suzuki, I. Kanno and H. Kotera, *Microsyst. Technol.*, 2007, **13**, 951–958.
13 W.-H. Tan and S. Takeuchi, *Adv. Mater.*, 2007, **19**, 2696–2701.
14 S. Utech, R. Prodanovic, A. S. Mao, R. Ostafe, D. J. Mooney and D. A. Weitz, *Adv. Healthcare Mater.*, 2015, **4**, 1628–1633.
15 D. M. G. Boggione, L. S. Batalha, M. T. P. Gontijo, M. E. S. Lopez, A. V. N. C. Teixeira, I. J. B. Santos and R. C. S. Mendonça, *Colloids Surf., B*, 2017, **158**, 182–189.
16 A. M. Chuah, T. Kuroiwa, I. Kobayashi, X. Zhang and M. Nakajima, *Colloids Surf., A*, 2009, **351**, 9–17.
17 C. M. E. Bitar, K. E. Markwick, D. Trelova, Z. Kroneková, M. Pelach, C. M. O. Selerier, J. Dietrich, I. Lacík and C. A. Hoesli, *Biotechnol. Prog.*, 2019, **35**, e2851.
18 S. Sugiura, T. Oda, Y. Izumida, Y. Aoyagi, M. Satake, A. Ochiai, N. Ohkohchi and M. Nakajima, *Biomaterials*, 2005, **26**, 3327–3331.
19 H. Huang, Y. Yu, Y. Hu, X. He, O. B. Usta and M. L. Yarmush, *Lab Chip*, 2017, **17**, 1913–1932.
20 Y. Deng, N. Zhang, L. Zhao, X. Yu, X. Ji, W. Liu, S. Guo, K. Liu and X. Z. Zhao, *Lab Chip*, 2011, **11**, 4117–4121.
21 S. Hong, H. J. Hsu, R. Kaunas and J. Kameoka, *Lab Chip*, 2012, **12**, 3277–3280.
22 H. Huang, M. Sun, T. Heisler-Taylor, A. Kiourti, J. Volakis, G. Lafyatis and X. He, *Small*, 2015, **11**, 5369–5374.
23 E. H. Wong, E. Rondeau, P. Schuetz and J. Cooper-White, *Lab Chip*, 2009, **9**, 2582–2590.
24 H. Huang and X. He, *Appl. Phys. Lett.*, 2014, **105**, 143704.
25 A. Hochstetter, R. Vernekar, R. H. Austin, H. Becker, J. P. Beech, D. A. Fedosov, G. Gompper, S.-C. Kim, J. T. Smith, G. Stolovizky, J. O. Tegenfeldt, B. H. Wunsch, K. K. Zeming, T. Krüger and D. W. Inglis, *ACS Nano*, 2020, **14**, 10784–10795.
26 K. J. Morton, K. Loutherback, D. W. Inglis, O. K. Tsui, J. C. Sturm, S. Y. Chou and R. H. Austin, *Lab Chip*, 2008, **8**, 1448–1453.
27 Y. Liu and T. Nisisako, *Biomicrofluidics*, 2022, **16**, 024101.
28 N. Tottori, T. Hatsuzawa and T. Nisisako, *RSC Adv.*, 2017, **7**, 35516–35524.
29 G. Ji, Y. Kanno and T. Nisisako, *Micromachines*, 2023, **14**, 622.
30 D. W. Inglis, *Appl. Phys. Lett.*, 2009, **94**, 013510.
31 Y. Liu, N. Tottori and T. Nisisako, *Sens. Actuators, B*, 2019, **283**, 802–809.
32 J. Lan, J. Chen, N. Li, X. Ji, M. Yu and Z. He, *Talanta*, 2016, **151**, 126–131.
33 F. Shao, L. Yu, Y. Zhang, C. An, H. Zhang, Y. Zhang, Y. Xiong and H. Wang, *Front. Bioeng. Biotechnol.*, 2020, **8**, 583065.
34 N. Tottori and T. Nisisako, *Sens. Actuators, B*, 2018, **260**, 918–926.
35 G. Ji, S. Masui, Y. Kanno and T. Nisisako, *Micromachines*, 2024, **15**, 908.
36 P. Agarwal, J. K. Choi, H. Huang, S. Zhao, J. Dumbleton, J. Li and X. He, *Part. Part. Syst. Charact.*, 2015, **32**, 809–816.
37 H. Aoki, Y. Masahiro, M. Xhimizu, Y. Hongoh, M. Ohkuma and Y. Yamagata, *Sci. Rep.*, 2022, **12**, 17014.